

Cathodic behavior of pure Al in sulfate media

N. Benzbiria,^{1,2*} T.T.M. Tran,³ M.W. Kendig,⁴ M. Zertoubi² and
W. Qafsaoui^{1*}

¹Laboratoire de l'Eau et de l'Environnement, Faculté des Sciences d'El Jadida, BP 20,
24000 El Jadida, Morocco

²Laboratoire Interface Matériaux et Environnement, Faculté des Sciences AinChock, BP
5366 Maârif, Casablanca, Morocco

³Sorbonne Université, CNRS, Laboratoire Interfaces et Systèmes Electrochimiques, 4 place
Jussieu, F-75005, Paris, France

⁴Kendig Research Associates LLC, 496 Hillsborough, Thousand Oaks, CA 91361, USA

*E-mail: wqafsaoui@gmail.com; nisrine.benzbiria@gmail.com

Abstract

The cathodic behavior of Al in 0.5 M Na₂SO₄ solution was studied by electrochemical methods. It was shown that the reduction of Fe(CN)₆³⁻ was difficult when an oxide layer was formed on the electrode surface during 1 h immersion in 0.5 M Na₂SO₄ solution due to the poor ionic and electronic conductivities of Al hydroxides. This reaction required a high cathodic overpotential on Al surface pre-treated at -2 V/SCE Al and was kinetically more difficult in comparison to platinum. Rotating disk electrode measurements showed that oxygen reduction reaction (ORR) was controlled by kinetics on both Al pre-treated at -2 V/SCE and oxidized Al cathodic dissolution was controlled by the supply of OH⁻ ions through H₂ evolution and by ORR on both oxidized Al electrode and the Al surface pre-treated at -2 V/SCE. Polarization curves obtained at different pH values showed that no dissolution behavior was observed at pH 5, whereas in neutral and alkaline solutions, OH⁻ ions production induced chemical dissolution of the hydroxide layer. In O₂ supersaturated solution, it was shown that ORR kinetics were slightly favored.

Keywords: aluminum, oxide film, cathodic corrosion, sulfate solution, polarization curves.

Received: April 22, 2019. Published: April 30, 2019

doi: [10.17675/2305-6894-2019-8-2-17](https://doi.org/10.17675/2305-6894-2019-8-2-17)

1. Introduction

Aluminum dissolution in aqueous neutral solutions has been extensively studied in the anodic domain where the oxide/hydroxide is insulating and exhibits a passive behavior [1–5]. Other studies have been conducted to investigate corrosion of aluminum alloys in some media where the metal undergoes galvanic corrosion [6–12]. In the technologically

important area of corrosion of micro-electronic devices, aluminum metallization has been shown to degrade primarily under conditions of cathodic bias [13, 14]. In general, aluminum is considered to be well protected from corrosive conditions and its dissolution rate remains very negligible, as long as its oxide film is undamaged [15, 16]. However, the passive layer cannot protect aluminum when it is polarized cathodically [17–22]. In fact, during oxygen and water reduction reactions, the generation of OH⁻ ions rises the local pH at the oxide/electrolyte interface, which induces aluminum oxide film solubility [4] and increases its dissolution rate. Therefore, Al electrodes undergo anodic dissolution and hydroxide deposition. This behavior assigned as cathodic corrosion [9, 23–26] has a major influence on the behavior of Al against corrosion in unbuffered neutral solutions or under environmental circumstances. Recent works have addressed the question in a quantitative way where the cathodic current and aluminum dissolution rate were estimated simultaneously. For instance, Despic *et al.* [27] studied the stoichiometry between hydrogen generated amount and the measured cathodic current and found that the hydrogen/electrons (H/e) ratio exhibited a value of 2 at low temperature due to the formation of monovalent aluminum species on the surface, while at high temperature a ratio of 4 was obtained explained by an increase in the portion of hydroxide leakage by mass-transfer. Baek *et al.* [28] used the quartz crystal microbalance technique to estimate aluminum dissolution rate, while the cathodic corrosion rate was determined by measuring H₂ evolution reaction (HER) through H₂O reduction. In the same perspective, Ogle *et al.* [24] measured aluminum dissolution rate during cathodic polarization by atomic emission spectroelectrochemistry (AESEC) under near steady state conditions. The authors stated that the Al dissolution was associated with the cathodic current, mainly the generation of the hydroxide formed at high cathodic potentials. The latter was followed then by aluminum oxidation, inducing repassivation of the surface.

The dissolution process goes through a sequence of both electrochemical and chemical reactions as given by the following reactions [24, 25]:



Therefore, the overall reaction can be written as:



Similarly, in a previous work [25] electrochemical methods were used to further elucidate the mechanism of cathodic dissolution of aluminum in 10^{-2} M Na_2SO_4 . On one hand, the measurement of interfacial pH during cathodic polarization showed that the pH reached a sufficiently high value at potentials more cathodic than -1.4 V/MSE (Saturated mercury sulfate electrode; $+0.645$ V/SHE) which was responsible for the oxide chemical dissolution. On the other hand, characterization of the oxide film in the potential range where it is stable (-1.325 V $< E < -1.03$ V/MSE) was carried out using electrochemical impedance spectroscopy. The oxide film thickness value was ranged between 8 and 9 nm in the potential region close to the open circuit potential E_{corr} , whereas at more negative potentials, the thickness dropped considerably due to the chemical dissolution of the passive film.

The present study considers the cathodic behavior of pure aluminum in 0.5 M Na_2SO_4 . The electrode surface reactivity was evaluated from the reduction polarization curves of $\text{Fe}(\text{CN})_6^{3-}$ ions. The electrochemical properties of an aluminum rotating disc electrode were studied as a function of surface state, pH and rotation rate.

2. Experimental

2.1. Materials

The working electrode consisted of an aluminum rotating-disk electrode (RDE) prepared from a pure aluminum cylinder rod (Goodfellow, 99.999% of quality) of 5 mm in diameter. The lateral part of the cylinder was covered with a cathaphoretic paint (PGG W975 + G323) to avoid the electrolyte infiltration in the lateral part of the cylinder rod. The rod was then embedded into an epoxy resin or a thermal shrinking sheath. The electrode surface was abraded before each experiment by rotating emery paper up to 1200 grade under water flow, and then rinsed abundantly with deionized water.

The reference electrode was a calomel electrode in saturated KCl (SCE; $+0.241$ V/ENH) and all the potentials measured were referred to SCE. The counter electrode was a platinum grid of large surface area set close to the cell wall.

Electrochemical tests were carried out on two surface conditions. On one hand, a cathodic polarization at -2 V/SCE was applied to the polished electrode for about 40 s in the working electrolyte itself [20]. This surface state will be designated as ‘pre-treated at -2 V surface’. On the other hand, the oxidized surface was obtained after immersion of the electrode in 0.5 M Na_2SO_4 solution. The open circuit potential (OCP) curves were recorded in order to select a suitable immersion time when the electrochemical system could reach a stable state.

Comparative measurements were conducted, in some conditions, on a platinum rotating disk electrode with a diameter of 1 mm, provided by Radiometer.

2.2. Electrolytes

Electrolytes were prepared from analytical grade chemicals (Sigma Aldrich) using distilled water. The measurements were performed in 0.5 M Na₂SO₄ (purity 99%) solution at pH 6.4. If necessary the pH was adjusted by addition of a dilute NaOH solution. The buffered solution at pH 5 was obtained by addition of sodium acetate (NaCH₃COO) and acetic acid (CH₃COOH).

Atmospheric oxygen served as the source of dissolved oxygen used in the electrochemical tests. In some cases, solutions were deoxygenated by purging for 30 minutes with nitrogen N₂ (purity 99.999%) or supersaturated by bubbling oxygen O₂ (99.999%) for 30 minutes. Both N₂ and O₂ gas were purchased from Air Liquide. Oxygen concentration was measured with Eutech's CyberScan 650 multi-parameter equipped with a Clark electrode. In air saturated and O₂ supersaturated media, the values of O₂ concentrations were 2×10^{-7} and 10^{-6} mol/cm³ respectively. In deaerated medium, O₂ concentration yielded a negligible value. During electrochemical runs, both purging and bubbling were continuously kept in the cell above the electrolyte.

In some cases, sodium sulfate solutions containing equal concentrations of K₄Fe(CN)₆ and K₃Fe(CN)₆ were prepared and used to initially study the reactivity of the surface towards Fe(CN)₆³⁻ reduction reaction.

2.3. Electrochemical measurements

Polarization measurements were carried out at 22°C in a conventional three-electrode cell. The working disk electrode faced towards the cell bottom. The cell was powered by a Voltalab PGZ 301 potentiostat/galvanostat.

Polarization curves were plotted at a potential scan rate of 0.5 mV/s and the influence of the electrode rotation rate was also studied. Three replica experiments were carried out for each experimental condition.

For the surface pre-treated at -2 V, the scanning direction was going from -2 V/SCE towards corrosion potential (E_{corr}). In the case of an oxidized aluminum surface, the polarization curves were recorded from E_{corr} towards -2 V/SCE.

3. Results and discussion

3.1. Electrochemical study of Fe(CN)₆³⁻ reduction on pure Al in deaerated 0.5 M Na₂SO₄

3.1.1. Influence of the potential scan rate on cathodic polarization curves

The cathodic polarization curve at -2 V of aluminum electrode in 0.5 M Na₂SO₄ solution is depicted in Figure 1a. After the pulse application, the current density becomes continuously negative due to H₂O and oxygen reduction reactions. Then, the current

density reaches a minimum of -6.69 mA/cm^2 . This leads to a chemical dissolution of Al surface film. Afterwards, the current direction is slowly reversed which may be related either to the accumulation of H_2 bubbles on the surface blocking the active sites, or to the fact that pH considerably increases locally which leads to the formation of an anodic product, such as hydroxides (most probably $\text{Al}(\text{OH})_3$). This current density deviation usually occurs after 40 s. Therefore, to avoid cathodic corrosion of the surface electrode, the polarization was held at -2 V during 40 s.

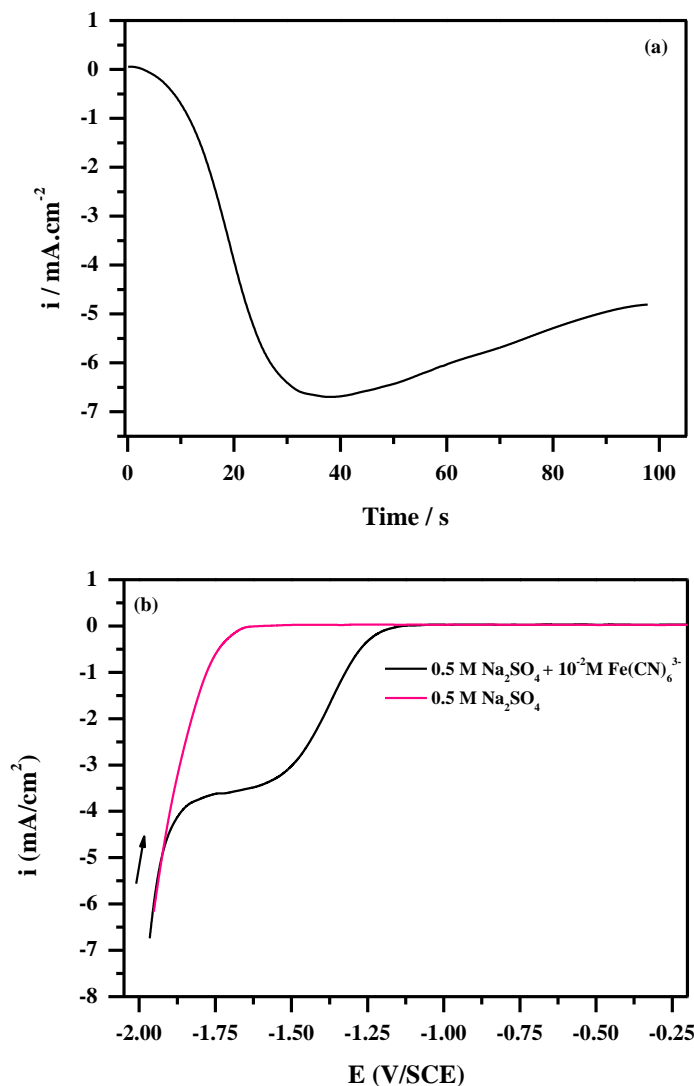


Figure 1. (a) Chronoamperometric measurement of pure aluminum electrode at -2 V/SCE at 0 rpm in air saturated $0.5 \text{ M Na}_2\text{SO}_4$ solution. (b) Cathodic polarization curves of Al electrode in deaerated $0.5 \text{ M Na}_2\text{SO}_4$ with and without $10^{-2} \text{ M Fe}(\text{CN})_6^{3-}/\text{Fe}(\text{CN})_6^{4-}$ at 1000 rpm (rotation per minute) and 0.5 mV/s . Scanning direction: $-2 \text{ V} \rightarrow E_{\text{corr}}$.

In order to assess removal of oxide, cathodic polarization curves were recorded just after surface polarization at -2 V in the presence and absence of $\text{Fe}(\text{CN})_6^{3-}$. This scanning was performed at 0.5 mV/s from -2 V to E_{corr} in deaerated 0.5 M Na_2SO_4 without and with 10^{-2} M $\text{Fe}(\text{CN})_6^{3-}/\text{Fe}(\text{CN})_6^{4-}$. The solution was deaerated to avoid oxygen reduction reaction (ORR) interference on $\text{Fe}(\text{CN})_6^{3-}$ reduction. In the absence of $\text{Fe}(\text{CN})_6^{3-}$ ions in the solution, Figure 1b shows that only H_2O reduction occurs at the beginning of the scan, around -1.8 V. However, in the solution containing 10^{-2} M $\text{Fe}(\text{CN})_6^{3-}/\text{Fe}(\text{CN})_6^{4-}$, H_2O reduction is followed by $\text{Fe}(\text{CN})_6^{3-}$ reduction reaction in the potential domain ranging from -1.7 to -1.57 V. Thus, one may claim that $\text{Fe}(\text{CN})_6^{3-}$ reduction does occur on Al surface but at higher overvoltages if compared to some earliest studies [29, 30].

In order to evaluate the influence of the potential scanning rate on the polarization curves, experiments were performed at 0.5 , 1 , 5 and 10 mV/s. Figure 2 presents the voltammograms recorded at different potential scan rates on aluminum electrode pretreated at -2 V in deaerated 0.5 M Na_2SO_4 solution containing 10^{-2} M $\text{Fe}(\text{CN})_6^{3-}/\text{Fe}(\text{CN})_6^{4-}$. The curves were drawn starting from -2 V to E_{corr} . In all cases, H_2O reduction occurs at about -1.8 V, followed by $\text{Fe}(\text{CN})_6^{3-}$ reduction plateau in the potential range going from -1.7 to -1.57 V. The only discrepancy is noticed in the charge transfer region, shown in the figure by the descending reduction wave. According to equation (7) [31], the kinetic current of a reaction limited by charge transfer is an exponential function of potential (V).

$$i_k = -k c_{\text{ox}}(\infty) \exp(-b_c V) \quad (7)$$

Where i_k is the kinetic current (A/cm^2), k is the kinetic constant (cm/s), $c_{\text{ox}}(\infty)$ is the bulk concentration and b_c is the cathodic Tafel slope ($b_c = \alpha n F / RT$) [31]. For instance, the charge transfer region at a scan rate of 10 mV/s starts from -1.41 to -0.68 V (730 mV), whereas at 0.5 mV/s, it goes from -1.53 to -1.2 V (330 mV). Thus, the overpotential required to overcome the kinetic regime at a scan rate of 10 mV/s is 2 times greater than the one required at 0.5 mV/s. As depicted in Figure 2, the charge transfer region narrows and the limited current plateau is well-defined at a scan rate of 0.5 mV/s if compared to the other curves recorded for higher scan rates. Thus, the study was conducted using a scan rate of 0.5 mV/s in order to favor the reduction kinetically and maintain steady state conditions at the electrode surface.

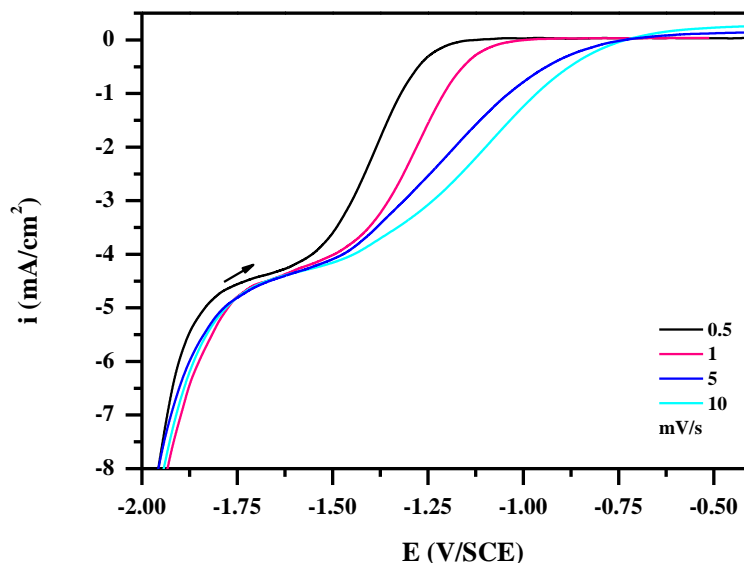


Figure 2. Cathodic polarization curves of Al electrode, at different potential scan rates, in deaerated 0.5 M Na_2SO_4 + 10^{-2} M $\text{Fe}(\text{CN})_6^{3-}/\text{Fe}(\text{CN})_6^{4-}$ at 1000 rpm. Scanning direction: $-2 \text{ V} \rightarrow E_{\text{corr}}$.

3.1.2. Cathodic polarization curves on Al pre-treated at -2 V , oxidized Al and Pt electrodes

In order to elucidate the influence of the Al native oxide film on ferricyanide ion reduction, polarization curves were recorded on Al pre-treated at -2 V and oxidized Al electrodes at 1000 rpm and at 0.5 mV/s , in deaerated $0.5 \text{ M Na}_2\text{SO}_4$ solution + $10^{-2} \text{ M Fe}(\text{CN})_6^{3-}/\text{Fe}(\text{CN})_6^{4-}$. The results were compared to those obtained on Pt. Note that for Pt and oxidized Al the scanning direction was started from E_{corr} to -2 V while for Al surface pre-treated at -2 V the potential sweep was carried out in the reverse direction (-2 V to E_{corr}). The results are shown in Figure 3.

On Pt electrode, H_2O reduction starts around -1 V , and a well-defined current density plateau due to diffusion limited ferricyanide reduction is observed between -0.9 V and -0.1 V , exhibiting a value of $-4.51 \text{ mA}\cdot\text{cm}^{-2}$ at -0.5 V . This is typical of platinum behavior towards ferricyanide reduction [29, 32].

On an aluminum surface pre-treated at -2 V , reduction of H_2O takes place at about -1.78 V , followed then by $\text{Fe}(\text{CN})_6^{3-}$ reduction in the region between -1.8 to -1.5 V , which is a higher overpotential than the one required on platinum. Moreover, this reaction takes place in a rather limited potential range ($\sim 300 \text{ mV}$) compared to that obtained on Pt ($\sim 800 \text{ mV}$). The current density plateau measured for Al pre-treated at -2 V (~ -4.33

mA/cm^2 at -1.6 V) and Pt ($\sim -4.51\text{ mA/cm}^2$ at -0.5 V) are relatively close, evidencing that one deals with the same process which is the diffusion-limited reduction of the ferricyanide species. The small difference noticed in the measured current densities is certainly due to the nature of the surface on which the reaction takes place.

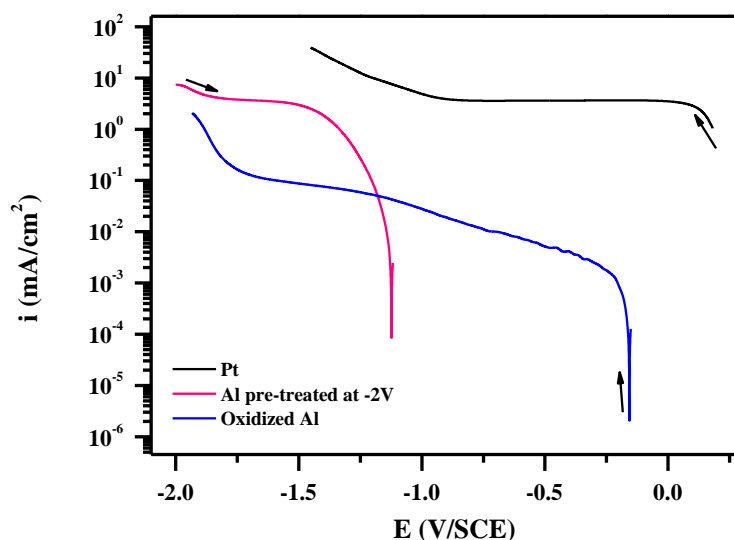


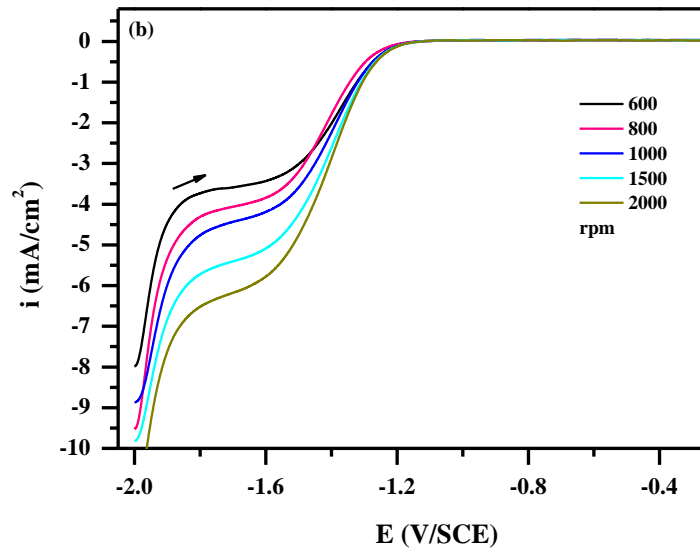
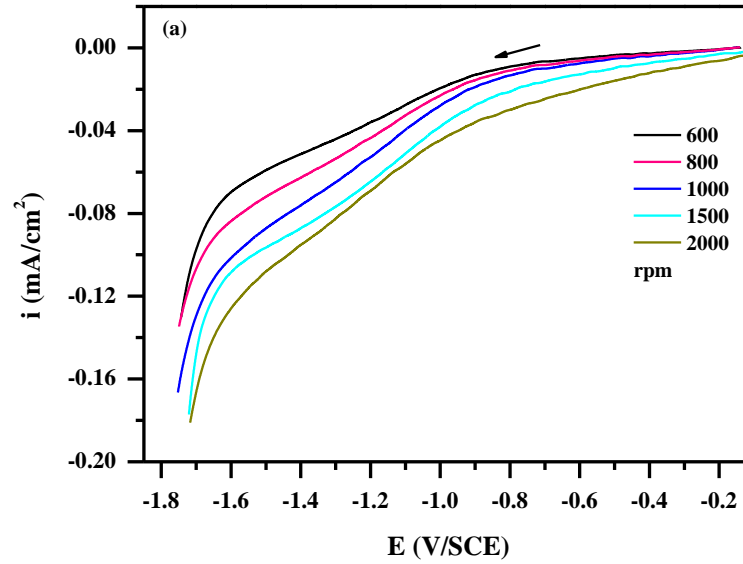
Figure 3. Cathodic polarization curves of Fe(CN)_6^{3-} reduction on Al pre-treated at -2 V , oxidized Al and on Pt in deaerated $0.5\text{ M Na}_2\text{SO}_4$ solution at 1000 rpm . Potential scan rate: 0.5 mV/s . Scanning direction: Pre-treated aluminum $-2\text{ V} \rightarrow E_{\text{corr}}$; Platinum and oxidized aluminum $E_{\text{corr}} \rightarrow -2\text{ V}$.

On an oxidized aluminum surface, Fe(CN)_6^{3-} reduction plateau is not observed. One can observe that the current density is reduced significantly exhibiting an insignificant value of -0.03 mA/cm^2 at a potential of -1 V . This indicates that the reaction rate is kinetically slow and difficult, which may be due to the high potential drop across the oxide layer [15, 25, 28] even for a common facile redox couple that is frequently used to access surface charge transfer kinetics.

The results obtained in this paragraph show that Fe(CN)_6^{3-} reduction is difficult on Al since the diffusion plateau is very restricted and the reaction requires very high overvoltages compared to that of Pt. The slow kinetics witnessed on Al are even more accentuated when the native oxide is present on the surface.

To further examine the kinetic parameters of ferricyanide ions reduction on oxidized Al, pre-treated Al at -2 V and Pt, representative potentiodynamic curves were recorded at various electrode rotation rates and at a scan rate of 0.5 mV/s in deaerated $0.5\text{ M Na}_2\text{SO}_4 +$

10^{-2} M $\text{Fe}(\text{CN})_6^{3-}/\text{Fe}(\text{CN})_6^{4-}$. Figure 4 presents the polarization curves obtained for oxidized Al (Figure 4a), Al pre-treated at -2 V (Figure 4b) and Pt (Figure 4c).



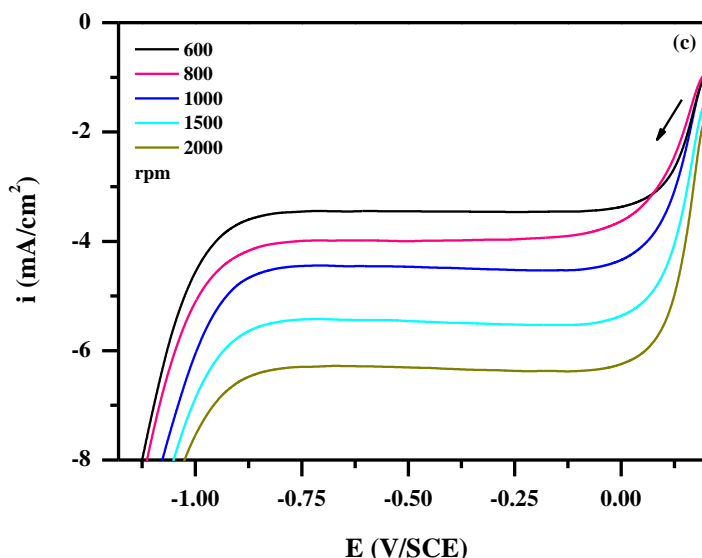


Figure 4. Electrochemical characterization of $\text{Fe}(\text{CN})_6^{3-}$ reduction on (a) oxidized Al ; (b) Al pre-treated at -2 V and (c) Pt in deaerated 0.5 M Na_2SO_4 solution. Potential scan rate: 0.5 mV/s. Scanning direction: Pre-treated Al -2 V \rightarrow E_{corr} ; Pt and oxidized Al $E_{\text{corr}} \rightarrow -2$ V.

From Figure 4a, it can be seen that when an oxide is developed on Al surface, the cathodic current densities slightly increase with rotation rate (ω), though no considerable difference was noted between the measured current densities for the different electrode rates. For instance, at a potential of -1.2 V, the current densities exhibit the values of -0.05 and -0.07 mA/cm^2 at a rotation rate of 600 and 1000 respectively. This indicates that ω has no significant influence on the cathodic current and thus the mass transfer regime is hardly reached likely due to the insulating character of the oxide surface film that disables electron transfer [28].

For Al pre-treated at -2 V (Figure 4b) and Pt (Figure 4c), the current densities increase gradually with electrode rotation rate, due to the shortened diffusion layer (δ_{ox}) as given by equation (8) [31].

$$i_{\text{lim}} = \frac{-nFD_{\text{ox}}c_{\text{ox}}(\infty)}{\delta_{\text{ox}}} \quad (8)$$

Where i_{lim} designates the mass transfer limited current density, n is the number of electrons transferred in accordance with the reaction stoichiometry, F is Faraday's constant and D_{ox} is the diffusion coefficient of ferricyanide ions.

Herein, the difference between a noble metal (Pt) where active sites are available and a reactive metal (Al) is clearly seen. In fact, in the case of Pt, the potential domain of the diffusion plateau remains practically the same even for high rotation rates. However, for Al pre-treated at -2 V, the limited current plateau tend to become more constrained when ω

increases. This is mainly due to the fact that the diffusion of $\text{Fe}(\text{CN})_6^{3-}$ ions is facilitated for higher ω values and then the charge transfer is considered as the rate determining step of the reduction process.

The limited current densities were measured for each electrode rotation rate to verify the Levich relationship given by equation (9) [33]:

$$i_d = 0.62nFc_{\text{ox}}(\infty)D_{\text{ox}}^{2/3}\nu^{-1/6}\omega^{1/2} \quad (9)$$

where i_d is the diffusion limited current density, ν is the kinematic viscosity (cm^2/s) and ω is the electrode rotation rate (rad/s).

Generally, in the case of faradaic reactions influenced by transport of the reacting species to the electrode surface, straight lines are obtained [31, 34, 35]. Therefore, determination of the electron number involved in the reaction can be determined from the slopes values. In this study, the Levich plots in Figure 5 (a and b) were drawn from potentials located in the middle of the current plateaus since the width of the potential range of the diffusion current plateaus is different for Pt and Al.

From Figure 5, it is noticeable that the limiting reduction currents follow the linear dependence on the square root of rotation rate on both Al pre-treated at -2 V and Pt. Hence, the use of Levich relationship is justified.

Using a set of data for ferricyanide concentration in the solution ($C = 10^{-5}$ mol/ cm^3), kinematic viscosity ($\nu = 1.009 \times 10^{-2}$ cm^2/s), and ferricyanide ion diffusivity ($D = 7 \times 10^{-6}$ cm^2/s) [32], the experimental values of n were determined and summarized in Table 1.

Furthermore, the lines fitted to the experimental data (Figure 5) exhibit a slope of 44.04×10^{-5} $\text{A}/\text{cm}^2 \text{s}^{-1/2}$ at a potential of -0.4 V and 38.46×10^{-5} $\text{A}/\text{cm}^2 \text{s}^{-1/2}$ at a potential of -1.65 V in the case of Pt and Al respectively. Therefore, the number of electron involved in the reaction is found to be close to 1, which is obviously due to the reduction of $\text{Fe}(\text{CN})_6^{3-}$ into $\text{Fe}(\text{CN})_6^{4-}$ following reaction (10):



From Figure 5b, one can see that the fitted lines obtained for Al pre-treated at -2 V yield non-zero intercept unlike the ones drawn for Pt. Hence, the reduction of $\text{Fe}(\text{CN})_6^{3-}$ ions is a mixed kinetic-diffusion process and subsequently obeyed the Koutecky-Levich equation [31,33] given by equation (11):

$$\frac{1}{i} = \frac{1}{i_d} + \frac{1}{i_k} = \frac{1}{B\omega^{1/2}} + \frac{1}{nFc_{\text{ox}}k} \quad (11)$$

B is a constant given by:

$$B = 0.62nFc_{\text{ox}}D^{2/3}\nu^{-1/6} \quad (12)$$

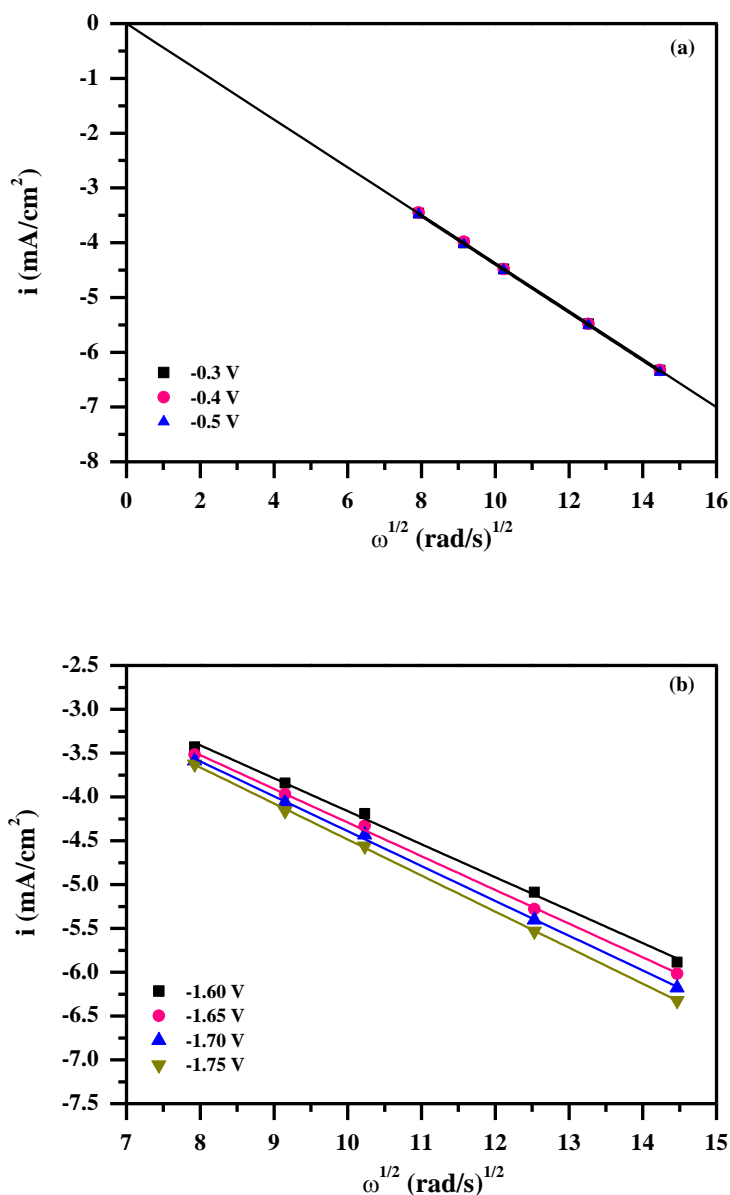


Figure 5. Levich Plots of $\text{Fe}(\text{CN})_6^{3-}$ reduction in deaerated Na_2SO_4 0.5 M solution on (a) Pt and (b) Al pre-treated at -2 V at various disk potentials.

In accordance with equation (11), the measured current density i involves two parameters: the current density limited by diffusion i_d , and the kinetic current density i_k .

The fact that the line obtained in the Levich plots passed through the zero intercept in the case of Pt, indicates that the total current is limited by pure diffusion. This is well known in the case of Pt as stated by several authors [36–39].

However in the case of Al pre-treated at -2 V, the kinetic current i_k and the heterogeneous reaction rate constant k can be determined on the basis of the linear relation between i^{-1} and $\omega^{-1/2}$.

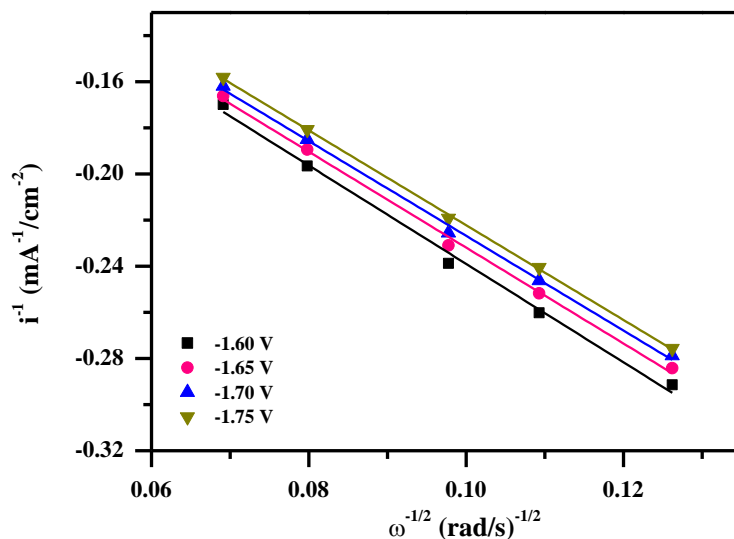


Figure 6. Koutecky–Levich plots of $\text{Fe}(\text{CN})_6^{3-}$ reduction in deaerated Na_2SO_4 0.5 M solution on Al electrode pre-treated at -2 V at various disk potentials.

Table 1. Kinetic parameters of $\text{Fe}(\text{CN})_6^{3-}$ reduction on Pt and Al pre-treated at -2 V determined using Levich and Koutecky–Levich plots.

	Disc Potential E (V/SCE)	Levich slope ($\times 10^{-5} \text{ A/cm}^2 \text{ s}^{-1/2}$)	n	i_k (A/cm^2)	k (cm/s)
Aluminum	-1.60	37.63	0.798	0.0390	0.051
	-1.65	38.46	0.815	0.0416	0.053
	-1.70	39.77	0.843	0.0466	0.057
	-1.75	41.14	0.872	0.0598	0.071
Platinum	-0.30	43.80	0.930	–	–
	-0.40	44.04	0.934	–	–
	-0.50	44.09	0.935	–	–

The Koutecky–Levich graphics (Figure 6) present straight and parallel lines attesting that both diffusion and charge transfer processes are involved in $\text{Fe}(\text{CN})_6^{3-}$ reduction reaction.

The kinetic contribution to the total current leads to a current density at the potential of -1.6 V of about 0.039 A/cm². This value is obtained from the intersection of the fitted line with the vertical axis in the Koutecky–Levich plot, which exhibits a kinetic constant of 0.051 cm/s.

Table 2 regroups values of rate constants (k) available in the literature for comparison purposes. In the current study, the rate constant obtained on Al pre-treated at -2 V is smaller than that on platinum. However, the value calculated (0.051 cm/s) is quite greater than the published ones of 10^{-3} M $\text{Fe}(\text{CN})_6^{3-}/\text{Fe}(\text{CN})_6^{4-}$ system on Nickel in 0.5 mol/dm³ KOH and defect free graphite in 1 M KCl.

Table 2. Values of rate constants k obtained on other electrode materials in different electrolytes at 25°C .

Electrode material	Electrolyte	$[\text{Fe}(\text{CN})_6^{3-}]$ (M)	k (cm/s)	Reference
Pt microdisc	1 M NaCl	5×10^{-4}	0.1–0.15	[40]
Pt microdisc	1 M KCl	5×10^{-4}	0.1–0.25	[40]
Pt	1 M KCl	10^{-2}	0.24	[29]
Bulk Nickel	0.5 M KOH	10^{-3}	3.8×10^{-3}	[30]
Defect free graphite	1 M KCl	10^{-3}	1.2×10^{-3}	[41]

From the results obtained in this section, it can be concluded that the reduction rate of ferricyanide ion is slow on Al surface pre-treated at -2 V if compared to a noble metal. Furthermore, the kinetics are significantly influenced by Al surface state as ferricyanide reduction is very difficult when Al native film is formed on the surface due to the high ionic and electronic resistance of Al passive film.

3.2. Cathodic investigation on Al surface in Na_2SO_4 0.5 M

After a preliminary study of the surface reactivity of pure Al towards $\text{Fe}(\text{CN})_6^{3-}$ reduction in deaerated medium, Al cathodic behavior in sodium sulfate solution is discussed in the section below.

3.2.1. Influence of aluminum surface state on polarization curves in air saturated 0.5 M Na_2SO_4 solution

It is now approved that cathodic reactions, and particularly ORR, are greatly influenced by several factors, including for instance the metal surface state. Earlier studies on a wide range of electrode materials have shown that on bare metal surfaces, oxygen is reduced directly to hydroxyl ions, whereas on oxidized surfaces ORR goes through the indirect pathway generating the formation of intermediates [42–45]. It is also interesting to mention

that in some cases ORR was found to proceed in a variety of combinations [43, 46, 47]. In fact, the reduction pathway depends on the chemical composition and the thickness of the oxide layer, which highly determines the number of active sites where oxygen can be preliminarily adsorbed, and affects automatically ORR kinetics.

Figure 7 shows E_{corr} evolution of pure Al electrode, during immersion time, at different rotation rates in air saturated 0.5 M Na_2SO_4 solution ($c_{\text{O}_2} = 2 \times 10^{-7} \text{ mol/cm}^3$). E_{corr} increases with time to reach a steady-state value after approximately one hour of immersion, which was accordingly chosen as the immersion time in this study. It can be noted that the steady state was achieved more rapidly when ω increases. This steady-state value was found to be about -1 V at 0 rpm and exhibited lower values for higher electrode rotation rates. The increase in open circuit potential value with time may result from the growth of a hydroxide layer on the surface electrode since the potential scan rate is slow.

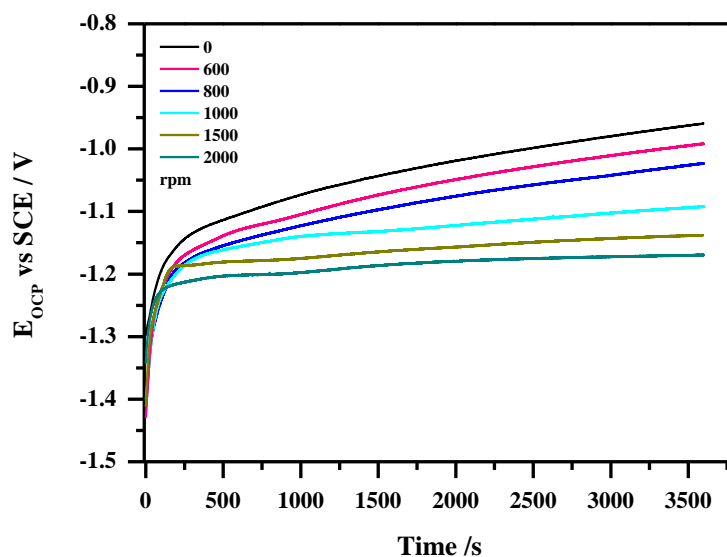


Figure 7. Open circuit potential evolution obtained for a pure Al electrode at various rotation rates going from 0 to 2000 rpm in air saturated 0.5 M Na_2SO_4 solution.

Figure 8a compares the behavior of aluminum electrode pre-treated at -2 V in air saturated 0.5 M Na_2SO_4 as the potential scan direction was reversed. It can be observed that when the polarization curve starts from E_{corr} towards -2 V , there is a considerable discrepancy in the potential range starting from -1.6 V to -2 V . It is also noticeable that the current density measured at a potential of -1.55 V is almost 3 times lower than that obtained when the scanning begins from more cathodic potentials towards E_{corr} . This may be related to the stability of Al passive film on the surface. When the scan is started from -2 V , Al hydroxide film is already destabilized by the large cathodic current generated

from H₂O reduction reaction and is replenishing as the potential is more anodic. As for the potential scan starting from E_{corr} , Al hydroxide film is more stable and thicker. It is noteworthy that even if the surface is subjected to a high cathodic polarization at -2 V, aluminum passive film is not entirely removed, since Al native hydroxide is inherently present on the surface. The few existing studies were dedicated to investigate the behavior of aluminum starting from E_{corr} [25, 48]. Therefore, it was worthwhile to conduct our study by scanning the potential from -2 V on Al surface pre-treated at -2 V, in order to avoid as much as possible the rapid formation of the oxide layer. Detailed views will be assessed by using RDE measurements on Al surface.

The influence of electrode rotation rate on the cathodic electrochemical behavior of Al was conducted in air saturated Na₂SO₄ 0.5 M solution for both Al pre-treated at -2 V and oxidized Al surfaces (Figures 8b and 8c). It is worthy to recall that the polarization curves are drawn from E_{corr} to -2 V for oxidized Al surface and from -2 V towards E_{corr} for the surface pre-treated at -2 V. Note that the total electrical current measured is the sum of the anodic current i_a related to Al dissolution (reaction (3)) and the cathodic current i_c [23]. The main cathodic reactions in neutral electrolyte are H₂O (reaction (1)) and O₂ reduction (reaction (2)). Each of these reactions leads to the formation of one OH⁻ per electron. Ogle *et al.* [24] measured the e/Al ratio and found it greater than 1, since a certain excess of hydroxide was required to compensate for diffusion of hydroxide away from the interfacial region. This indicates that the concentration of OH⁻ at the interface and the variation of cathodic dissolution rate are simply related to the cathodic current rather than potential [23].

On a surface pre-treated at -2 V (Figure 8b), three different behaviors can be observed:

- The potential range more negative than -1.60 V is attributed likely to H₂O reduction (I). Serdechnova *et al.* [23] investigated AA6061 alloy dissolution in 3% NaCl solution by scanning the potential from -1.78 to -0.6 V *vs.* SCE at 1 mV/s and revealed that Al cathodic dissolution was clearly observed, and the current approached a value of -6 to -8 mA/cm² near -1.78 V *vs.* SCE and decreased drastically as the potential becomes increasingly anodic. The authors also indicated that Al dissolution rate was a maximum near -1.73 V *vs.* SCE and decreased simultaneously with the cathodic current. From these observations, it can be suggested that in this potential range Al hydroxide is damaged by OH⁻ ions production through H₂O reduction.
- In the region between -1.60 and -1.35 V, chemical dissolution of the oxide due to local pH increase, followed by aluminum anodic dissolution and hydroxide deposition are probably occurring along with oxygen reduction reaction [25] (II).
- In the potential domain going from -1.35 V to -1.2 V, oxygen is expected to be reduced [25] (III).

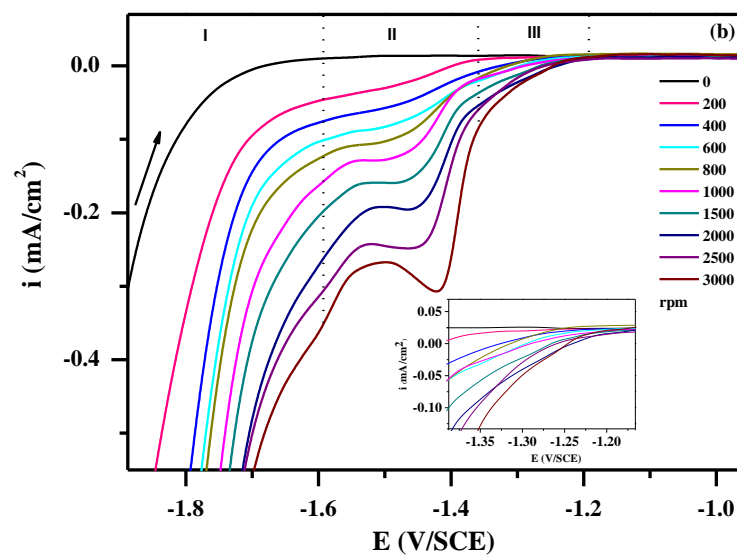
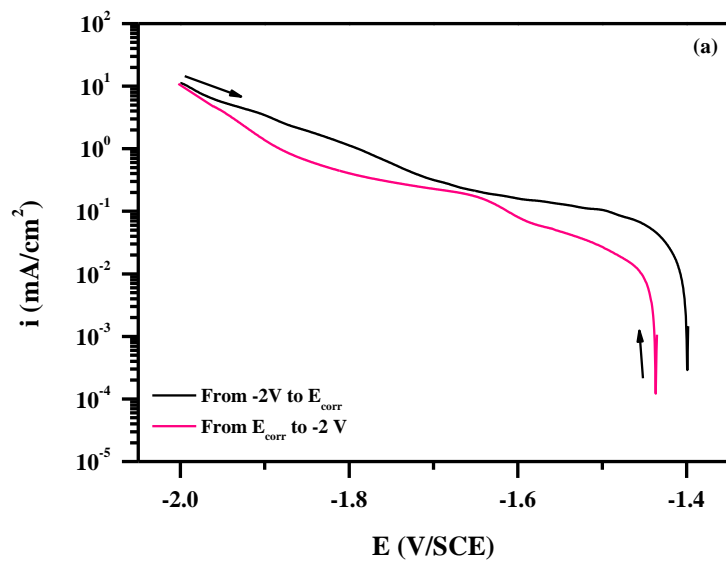
In region (I), the local pH starts to increase mainly due to HER. As for region (II), the total current is the sum of both cathodic (ORR) and anodic contributions (Al cathodic corrosion). In this potential domain, the increase of ω facilitates O₂ supply to the electrode surface where it can be reduced to OH⁻. Therefore, at 3000 rpm, the pH becomes locally more alkaline and the anodic contribution to the total current is greater. This can explain the presence of the hump on the polarization curve presented in Figure 8b. Subsequently, when the potential is scanned towards more anodic values, the local pH tend to decrease and Al anodic dissolution rate declines as well. As a result, the ORR contribution to the total current becomes more important which leads to the increase in the cathodic current.

In fact, Serdechnova *et al.* [23] work showed that aluminum dissolution occurs based on a simple model where hydroxide generation, Al(OH)₃ formation/dissolution and Al(OH)₄⁻ diffusion are kinetically coupled. They also revealed that Al cathodic corrosion was linearly proportional to the hydroxide generation rate. Accordingly, they reported that the instantaneous dissolution rate had a stoichiometry of OH⁻/Al³⁺ of 1.62±0.22 in the case of 99.99% Al.

Regarding ORR potential domain, as depicted in the insert of Figure 8b, no defined current plateaus are noticeable, which indicates that the charge transfer is a low process and is considered as the rate limiting step. This is in accordance with other works, showing that electron transfer is the limiting step of ORR on pure Al surface [25, 28, 48].

Figure 8c shows the RDE curves drawn from E_{corr} on an oxidized surface in air saturated solution. It can be seen that ORR takes place on the potential range going from -1.27 V until the end of the scan and is clearly kinetically controlled as seen in the insert of Figure 8c, since no current plateau is observed and no influence of rotation rate on the measured current densities is witnessed. It is now endorsed that ORR is sluggish and is kinetically difficult on Al surface, mainly when the oxide layer is present on the surface due to the ohmic behavior of the developed film [25, 28]. In a previous work [25] the estimated value of the layer film resistance (R_{film}) was about $2 \times 10^4 \Omega \text{ cm}^2$.

The cathodic current continues to increase until the potential scan reaches a value of -1.47 V. However, at potentials more cathodic than -1.47 V, OH⁻ production by ORR raised the interfacial pH and causes dissolution of the passive film as indicated by the thermodynamic calculations [49]. In this case, the anodic contribution to the total current tend to become higher than the cathodic one, explaining the decrease of the cathodic current (observed from -1.47 V to -1.55 V) and the presence of a constant current in the potential domain going from -1.57 V to -1.90 V. This behavior is likely related to the increase of Al anodic dissolution rate. For potentials more cathodic than -1.90 V, H₂O is reduced on the altered hydroxide layer Al(OH)₃ [25].



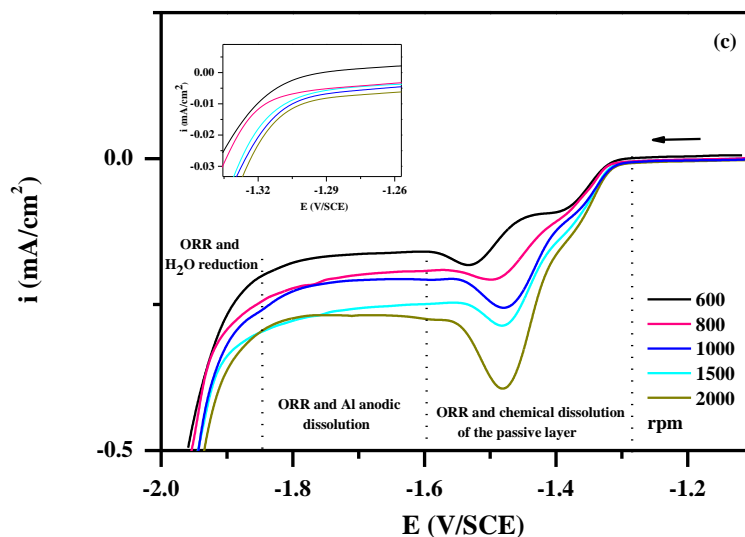


Figure 8. Cathodic polarization curves on Al in air saturated 0.5 M Na_2SO_4 solution: (a) Comparison between the curves recorded at different scanning direction at 1000 rpm; (b) RDE measurements on Al pre-treated at -2 V and (c) oxidized Al, scan potential rate: 0.5 mV/s, scanning direction: Pre-treated Al -2 V \rightarrow E_{corr} ; Oxidized Al E_{corr} \rightarrow -2 V.

3.2.2. pH influence on the cathodic behavior of Al in air saturated 0.5 M Na_2SO_4

In order to assess the pH influence on the cathodic currents, potentiodynamic curves were recorded on Al pre-treated at -2 V for different pH values of Na_2SO_4 solutions at a rotation rate of 1000 rpm. As shown in Figure 9, the cathodic curve obtained at pH 5 shows no dissolution plateau. Similar results were obtained on an oxidized Al surface. In acidic solution, the cathodic current is predominantly generated by H_2O reduction and ORR. According to Cabot *et al.* [20], the acidity of the solution maintains the presence of the passive layer on aluminum surface even at higher negative potentials. In this case, Al cathodic corrosion is prevented and one can suggest that ORR takes place on an unmodified oxide layer. Taking this into account, cathodic Tafel slope values were estimated from the corresponding polarization curves at pH 5. In the -1.3 to -1.6 potential range, the slopes yield values of 270 mV/decade and 302 mV/decade on Al pre-treated at -2 V and oxidized Al surfaces respectively. Therefore, aluminum surface is considered less reactive towards cathodic reactions, particularly when the electrode is covered with a stable Al oxide layer, which is known to exhibit poor ionic and electronic conductivities.

Several studies were conducted on the behavior of Al in aqueous solutions at different pH values. Metikos-Hukovic *et al.* [50] stated that the cathodic Tafel slope yielded a value of 224 mV/decade in 0.5 M HCl solution, while Metikos-Hukovic *et al.* [51] estimated a value of 238 mV/decade in 1 M HClO_4 solution. In a buffered solution at pH 7 [25], a

value of 260 mV/decade was obtained for the cathodic Tafel slope calculated where ORR occurred at a homogenous Al oxide. From these results, one may assume that the presence of Al oxide film influences the reduction mechanism either by creating a barrier to charge transfer process or by altering the energetics of the cathodic reaction at the double layer [50].

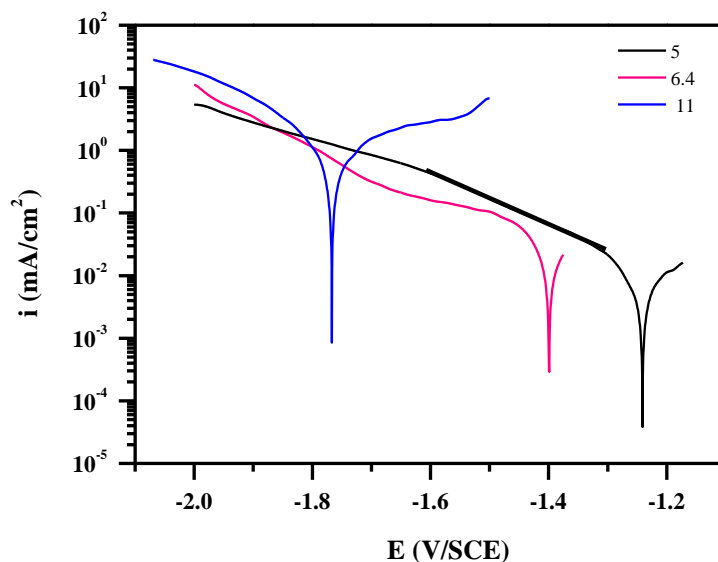


Figure 9. Polarization curves of aluminum electrode pre-treated at -2 V in air saturated 0.5 M Na_2SO_4 solution at different pH at 1000 rpm. Potential scan rate: 0.5 mV/s. The scanning direction: -2 V \rightarrow E_{corr} .

However, when the pH is much higher (~ 11), it is noticeable that E_{corr} is shifted towards very negative values (-1.77 V) if compared, for instance to the one observed for a surface pre-treated at -2 V in sulfate solution at pH 6.4. Note also that there was a generation of an anodic current over a wide potential domain, more cathodic than the E_{corr} measured at lower pH values. Similar results were found on an oxidized surface (not shown). This behavior points out that the alkalization of the interface Al/solution, due to pH increase, causes oxide chemical dissolution and favors anodic dissolution of aluminum [4]. Several authors reported identical behavior in alkaline solutions [9, 23–25]. In a previous study [25] conducted in 10^{-2} M Na_2SO_4 adjusted to pH 11, E_{corr} was shifted very cathodically (-1.65 V/MSE) and an anodic current was noticed at negative potential values. Mokaddem *et al.* [9] used atomic emission spectroelectrochemistry (AESEC) to monitor the dissolution of Al in 30 g/L NaCl solution as a function of pH. They showed that in alkaline solution (pH = 11.8), no passivation phenomenon was observed, and the anodic dissolution of aluminum was detected in the whole studied potential region.

Similarly, it was reported by Zhang *et al.* [4] that aluminate ions $\text{Al}(\text{OH})_4^-$ are the only stable form of aluminum in alkaline solutions, and the solubility of the oxide increases with pH increasing.

3.2.3. ORR process on pure Al

Figure 10 shows the cathodic polarization curves recorded at different O_2 concentration in the solution and at a rotation rate of 1000 rpm of Al electrode. In the deaerated solution, reduction of H_2O is the only reaction observed and it occurs beyond -1.7 V. E_{corr} is close to -1.68 V.

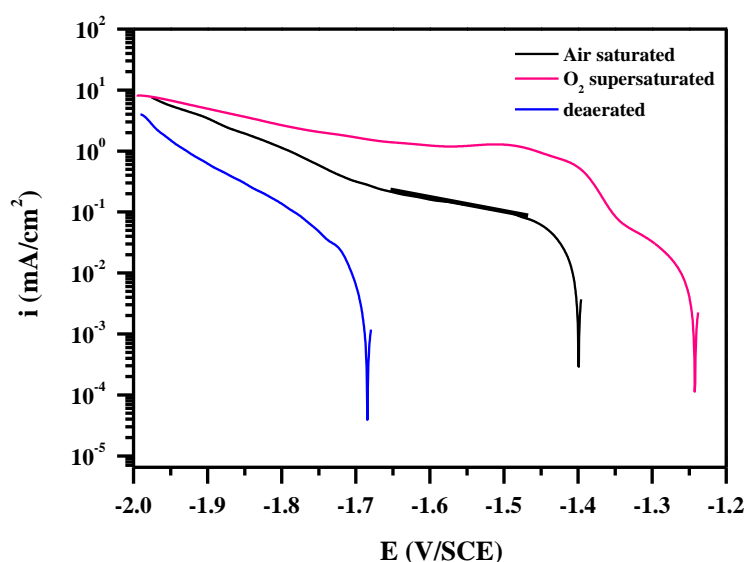


Figure 10. Polarization curves of Al pre-treated at -2 V in 0.5 M Na_2SO_4 solution for different O_2 concentrations at 1000 rpm. Potential sweep rate: 0.5 mV/s. Scanning direction: -2 V \rightarrow E_{corr} .

In air saturated Na_2SO_4 solution ($c_{\text{O}_2} = 2 \times 10^{-7}$ mol/cm³), E_{corr} exhibits a value of -1.39 V and the charge transfer region extends over a potential domain of 100 mV (from -1.4 to -1.6 V). The Tafel behavior observed in the -1.45 to -1.6 V potential range, presents b_c values of 318 and 350 mV/decade on pre-treated at -2 V and oxidized Al surfaces respectively. This increase of Tafel slope value by 32 mV/decade reveals that ORR kinetics are more slower when the passive film is developed on Al surface.

In O_2 supersaturated sulfate solution ($c_{\text{O}_2} = 10^{-6}$ mol/cm³), the charge transfer region becomes narrower (from -1.25 to -1.34 V) and E_{corr} is shifted towards more anodic potentials than in air saturated medium, which suggests that the ORR is favored in O_2

supersaturated Na_2SO_4 solution. Cathodic Tafel slopes were not estimated in this case, due to the fluctuation of oxygen concentration during potentiodynamic polarization.

In other works conducted on the study of ORR on platinum, palladium, rhodium [52], zinc [35] and copper electrodes [53], a Tafel slope of 120 mV/decade was obtained at high cathodic polarization and a value of 60 mV/decade at lower polarizations. However, Al behaves very differently, which indicates that Al electrode is a very inactive cathode regarding the mechanistic implications of O_2 reduction. In all cases, charge transfer rate is low and remains the rate determining step for ORR in sodium sulfate solution despite the pH value.

4. Conclusions

Through this study on the cathodic behavior of Al surface in neutral sulfate medium several interesting results were highlighted and can be listed as follows:

- Reduction of ferricyanide ion requires a high cathodic overpotential on Al surface pre-treated at -2 V and is kinetically more difficult if compared to platinum. It is even more difficult on the oxide layer formed during 1 hour immersion in 0.5 M Na_2SO_4 solution. This reaction requires a high cathodic overpotential on Al surface pre-treated at -2 V and is kinetically more difficult if compared to platinum. The number of electrons exchanged is about 1 as expected, the kinetic current i_k is found to be around 0.0345 A/cm^2 and the kinetic constant k yields a value of 0.044 cm/s at a potential of -1.6 V.
- Al cathodic dissolution is controlled by the cathodic current and thus by the supply of OH^- through H_2 evolution and by ORR on both Al surface pre-treated at -2 V and oxidized Al electrode.
- In a buffered solution at pH 5, ORR occurs on an unmodified oxide layer since no dissolution behavior was observed. However, at pH 11, E_{corr} shifts towards very negative values, accompanied with the generation of an anodic current. Al/solution interface alkalization due to pH increase, causes oxide chemical dissolution and favors anodic dissolution of Al.
- ORR at Al surface is a process controlled by kinetics and diffusion regime is never obtained, even on Al pre-treated at -2 V, due to the high potential drop across the oxide layer.

References

1. O. Guseva, P. Schmutz, T. Suter and O. von Trzebiatowski, *Electrochim. Acta*, 2009, **54**, 4514–4524. doi: [10.1016/j.electacta.2009.03.048](https://doi.org/10.1016/j.electacta.2009.03.048)
2. M. Verhoff and R. Alkire, *J. Electrochem. Soc.*, 2000, **147**, no. 4, 1349–1358. doi: [10.1149/1.1393362](https://doi.org/10.1149/1.1393362)
3. F.J. Martin, G.T. Cheek, W.E. O’Grady and P.M. Natishan, *Corros. Sci.*, 2005, **47**, no. 12, 3187–3201. doi: [10.1016/j.corsci.2005.05.058](https://doi.org/10.1016/j.corsci.2005.05.058)
4. J. Zhang, M. Klasky and B.C. Letellier, *J. Nucl. Mater.*, 2009, **384**, 175–189. doi: [10.1016/j.jnucmat.2008.11.009](https://doi.org/10.1016/j.jnucmat.2008.11.009)
5. H.J.W. Lenderink, M.V.D. Linden and J.H.W. De Wit, *Electrochim. Acta*, 1993, **38**, no. 14, 1989–1992. doi: [10.1016/0013-4686\(93\)80329-X](https://doi.org/10.1016/0013-4686(93)80329-X)
6. W. Qafsaoui, M.W. Kendig, H. Perrot and H. Takenouti, *Corros. Sci.*, 2015, **92**, 245–255. doi: [10.1016/j.corsci.2014.12.011](https://doi.org/10.1016/j.corsci.2014.12.011)
7. T. Suter and R.C. Alkire, *J. Electrochem. Soc.*, 2001, **148**, no. 1, B36–B42. doi: [10.1149/1.1344530](https://doi.org/10.1149/1.1344530)
8. N. Birbilis and R.G. Buchheit, *J. Electrochem. Soc.*, 2005, **152**, no. 4, B140–B151. doi: [10.1149/1.1869984](https://doi.org/10.1149/1.1869984)
9. M. Mokaddem, P. Volovitch, F. Rechou, R. Oltra and K. Ogle, *Electrochim. Acta*, 2010, **55**, 3779–3786. doi: [10.1016/j.electacta.2010.01.079](https://doi.org/10.1016/j.electacta.2010.01.079)
10. A. Schussler and H.E. Exner, *Corros. Sci.*, 1993, **34**, no. 11, 1803–1815. doi: [10.1016/0010-938X\(93\)90018-C](https://doi.org/10.1016/0010-938X(93)90018-C)
11. J.-B. Jorcin, C. Blanc, N. Pébère, B. Tribollet and V. Vivier, *J. Electrochem. Soc.*, 2008, **155**, no. 1, C46. doi: [10.1149/1.2803506](https://doi.org/10.1149/1.2803506)
12. S.V. Oleynik, V.S. Rudnev, Y.A. Kuzenkov, T.P. Jarovaja, L.F. Trubetskaja and P.M. Nedorozov, *Int. J. Corros. Scale Inhib.*, 2017, **6**, no. 2, 91–111. doi: [10.17675/2305-6894-2017-6-2-1](https://doi.org/10.17675/2305-6894-2017-6-2-1)
13. M. Kendig, M. Abdel-Gawad and R. Addison, *Corrosion*, 1992, **48**, no. 4, 368–372. doi: [10.5006/1.3315946](https://doi.org/10.5006/1.3315946)
14. J.W. Osenbach, *Semicond. Sci. Technol.*, 1996, **11**, 155–162. doi: [10.1088/0268-1242/11/2/002](https://doi.org/10.1088/0268-1242/11/2/002)
15. D.D. Eley and P.R. Wilkinson, *Proc. R. Soc. A Math. Phys. Eng. Sci.*, 1960, **254**, no. 1278, 327–342. doi: [10.1098/rspa.1960.0023](https://doi.org/10.1098/rspa.1960.0023)
16. J.O.M. Bockris and L.V. Minevski, *J. Electroanal. Chem.*, 1993, **349**, no. 1–2, 375–414. doi: [10.1016/0022-0728\(93\)80186-L](https://doi.org/10.1016/0022-0728(93)80186-L)
17. Y.S. Kim, S.I. Pyun, S.M. Moon and J.D. Kim, *Corros. Sci.*, 1996, **38**, no. 2, 329–336. doi: [10.1016/0010-938X\(96\)00131-X](https://doi.org/10.1016/0010-938X(96)00131-X)

18. S.M. Moon and S.I. Pyun, *Corros. Sci.*, 1997, **39**, no. 2, 399–408. doi: [10.1016/S0010-938X\(97\)83354-9](https://doi.org/10.1016/S0010-938X(97)83354-9)
19. K. Azumi, T. Ueno and M. Seo, *J. Electroanal. Chem.*, 2004, **567**, 1–7. doi: [10.1016/j.jelechem.2003.11.057](https://doi.org/10.1016/j.jelechem.2003.11.057)
20. P.L.L. Cabot, J.A. Garrido, E.P. Rez and J. Virgili, *Corros. Sci.*, 1986, **26**, no. 5, 357–369. doi: [10.1016/0010-938X\(86\)90011-9](https://doi.org/10.1016/0010-938X(86)90011-9)
21. H. Takahashi, K. Fujiwara and M. Seo, *Corros. Sci.*, 1994, **36**, no. 4, 689–705. doi: [10.1016/0010-938X\(94\)90074-4](https://doi.org/10.1016/0010-938X(94)90074-4)
22. G.T. Burstein and C. Liu, *Corros. Sci.*, 1995, **37**, no. 7, 1151–1162. doi: [10.1016/0010-938X\(95\)00023-D](https://doi.org/10.1016/0010-938X(95)00023-D)
23. M. Serdechnova, P. Volovitch, F. Brisset and K. Ogle, *Electrochim. Acta*, 2014, **124**, 9–16. doi: [10.1016/j.electacta.2013.09.145](https://doi.org/10.1016/j.electacta.2013.09.145)
24. K. Ogle, M. Serdechnova, M. Mokaddem and P. Volovitch, *Electrochim. Acta*, 2011, **56**, no. 4, 1711–1718. doi: [10.1016/j.electacta.2010.09.058](https://doi.org/10.1016/j.electacta.2010.09.058)
25. T.T.M. Tran, B. Tribollet and E.M.M. Sutter, *Electrochim. Acta*, 2016, **216**, 58–67. doi: [10.1016/j.electacta.2016.09.011](https://doi.org/10.1016/j.electacta.2016.09.011)
26. B.P. Caldwell and V.J. Albano, *Trans. Electrochem. Soc.*, 1939, **76**, no. 1, 271–285. doi: [10.1149/1.3500282](https://doi.org/10.1149/1.3500282)
27. A.R. Despić, J. Radošević, P. Dabić and M. Kliškić, *Electrochim. Acta*, 1990, **35**, no. 11–12, 1743–1746. doi: [10.1016/0013-4686\(90\)87074-C](https://doi.org/10.1016/0013-4686(90)87074-C)
28. Y. Baek and G.S. Frankel, *J. Electrochem. Soc.*, 2003, **150**, no. 1, B1–B9. doi: [10.1149/1.1524172](https://doi.org/10.1149/1.1524172)
29. P.H. Daum and C.G. Enke, *Anal. Chem.*, 1969, **41**, no. 4, 653–656. doi: [10.1021/ac60273a007](https://doi.org/10.1021/ac60273a007)
30. D.A. Szanto, S. Cleghorn, C. Ponce-de-León and F.C. Walsh, *AIChE J.*, 2008, **54**, no. 3, 802–810. doi: [10.1002/aic.11420](https://doi.org/10.1002/aic.11420)
31. M.T.T. Tran, B. Tribollet, V. Vivier and M.E. Orazem, *Russ. J. Electrochem.*, 2017, **53**, no. 9, 932–940. doi: [10.1134/S1023193517090142](https://doi.org/10.1134/S1023193517090142)
32. P. Kulesza, T. Jedral and Z. Galus, *J. Electroanal. Chem.*, 1980, **109**, no. 1–3, 141–149. doi: [10.1016/S0022-0728\(80\)80112-4](https://doi.org/10.1016/S0022-0728(80)80112-4)
33. A. Bard and L. Faulkner, *Electrochemical Methods*, 1980.
34. M.B. Vukmirovic, N. Vasiljevic, N. Dimitrov and K. Sieradzki, *J. Electrochem. Soc.*, 2003, **150**, no. 1, B10. doi: [10.1149/1.1526554](https://doi.org/10.1149/1.1526554)
35. H. Dafydd, D.A. Worsley and H.N. McMurray, *Corros. Sci.*, 2005, **47**, 3006–3018. doi: [10.1016/j.corsci.2005.05.036](https://doi.org/10.1016/j.corsci.2005.05.036)
36. N.M. Markovic, H.A. Gasteiger and P.N. Ross, *J. Phys. Chem.*, 1995, **99**, no. 11, 3411–3415. doi: [10.1021/j100011a001](https://doi.org/10.1021/j100011a001)

-
37. M.D. Maciá, J.M. Campiña, E. Herrero and J.M. Feliu, *J. Electroanal. Chem.*, 2004, **564**, 141–150. doi: [10.1016/j.jelechem.2003.09.035](https://doi.org/10.1016/j.jelechem.2003.09.035)
38. B. Wang, *J. Power Sources.*, 2005, **152**, 1–15. doi: [10.1016/j.jpowsour.2005.05.098](https://doi.org/10.1016/j.jpowsour.2005.05.098)
39. L. Ma, C. Wang, B.Y. Xia, K. Mao, J. He, X. Wu, Y. Xiong and X.W. Lou, *Angew. Chem., Int. Ed.*, 2015, **54**, 1–7. doi: [10.1002/anie.201500947](https://doi.org/10.1002/anie.201500947)
40. C. Beriet and D. Pletcher, *J. Electroanal. Chem.*, 1993, **361**, 93–101. doi: [10.1016/0022-0728\(93\)87042-T](https://doi.org/10.1016/0022-0728(93)87042-T)
41. A.T. Valota, I.A. Kinloch, K.S. Novoselov, C. Casiraghi, A. Eckmann, E.W. Hill and R.A.W. Dryfe, *ACS Nano*, 2011, **5**, no. 11, 8809–8815. doi: [10.1021/nn202878f](https://doi.org/10.1021/nn202878f)
42. N. Le Bozec, C. Compère, M. L’Her, A. Laouenan, D. Costa and P. Marcus, *Corros. Sci.*, 2001, **43**, no. 4, 765–786. doi: [10.1016/S0010-938X\(00\)00113-X](https://doi.org/10.1016/S0010-938X(00)00113-X)
43. M.V. Vazquez, S.R. de Sanchez, E.J. Calvo and D.J. Schiffrin, *J. Electroanal. Chem.*, 1994, **374**, no. 1–2, 189–197. doi: [10.1016/0022-0728\(94\)03343-9](https://doi.org/10.1016/0022-0728(94)03343-9)
44. V. Jovancicevic and J.O.M. Bockris, *J. Electrochem. Soc.*, 1986, **133**, no. 9, 1797–1807. doi: [10.1149/1.2109021](https://doi.org/10.1149/1.2109021)
45. N.M. Markovic, T.J. Schmidt, V. Stamenkovic and P.N. Ross, *Fuel Cells*, 2001, **1**, no. 2, 105–116.
46. T.D. Daff, D. Costa, I. Lisiecki and N.H. De Leeuw, *J. Phys. Chem. C.*, 2009, **113**, no. 35, 15714–15722. doi: [10.1021/jp904054n](https://doi.org/10.1021/jp904054n)
47. F. King, M.J. Quinn and C.D. Litke, *J. Electroanal. Chem.*, 1995, **385**, 45–55. doi: [10.1016/0022-0728\(94\)03705-8](https://doi.org/10.1016/0022-0728(94)03705-8)
48. G.O. Ilevbare and J.R. Scully, *Corrosion*, 2001, **57**, no. 2, 134–152. doi: [10.5006/1.3290339](https://doi.org/10.5006/1.3290339)
49. M. Pourbaix, *Atlas of Electrochemical Equilibria in Aqueous Solutions*, NACE International, Houston, Texas; Cebelcor, Brussels, 1966.
50. M. Metikos-Hukovic, R. Babic and Z. Grubac, *J. Appl. Electrochem.*, 2002, **32**, 35–41. doi: [10.1023/A:1014265407060](https://doi.org/10.1023/A:1014265407060)
51. M. Metikos-Hukovic, Z. Grubac and E. Stupnisek-Lisac, *Corrosion*, 1994, **50**, no. 2, 146–151. doi: [10.5006/1.3293503](https://doi.org/10.5006/1.3293503)
52. M.R. Tarasevic, *Comprehensive Treatise of Electrochemistry*, Vol. 10, 1985.
53. T. Jiang and G.M. Brisard, *Electrochim. Acta*, 2007, **52**, no. 13, 4487–4496. doi: [10.1016/j.electacta.2006.12.044](https://doi.org/10.1016/j.electacta.2006.12.044)

